Multi-period Fast Robust Optimization of Distribution System With Cables

Jian Zhang [1] and Mingjian Cui [2,2]

[1]Affiliation not available
[2]The University of Tennessee

November 8, 2023

Abstract

In the existing multi-period robust optimization method of active and reactive power coordination in distribution networks, the reactive power regulation capability of distributed generators (DGs), operation costs of regulating equipment, and the current of shunt capacitance of cables are not taken into account. In this paper, based on branch flow equations, a multi-period two-stage mixed integer second-order cone programming (SOCP) robust optimization model of active and reactive coordination in distribution system with cables is developed considering the reactive power regulation capability of DG, action costs of switched capacitor reactor (SCR), on load tap changer transformer (OLTC), energy storage system (ESS), and current of shunt capacitor of cables. Further, against to the deficiency of low computational rate of column and constraint generation method (CCG), a novel method iteratively solving the first and second stage model on cutting plane is proposed. In the first stage model, the number of variables and constraints keeps constant during the iteration. In the second stage model, it only needs to solve the model of each single time period. Then their results are accumulated. Thus, the computational speed using the proposed method is much higher than CCG. The effectiveness of the proposed method is separately validated on the 4-bus, IEEE 33-bus, and PG69-bus distribution systems.

Multi-Period Fast Robust Optimization of Distribution System With Cables

Jian Zhang, Mingjian Cui, *Senior Member, IEEE*, Yigang He, *Member, IEEE*, and Fangxing Li, *Fellow, IEEE*

Abstracts—In the existing multi-period robust optimization method of active and reactive power coordination in distribution networks, the reactive power regulation capability of distributed generators (DGs), operation costs of regulating equipment, and the current of shunt capacitance of cables are not taken into account. In this paper, based on branch flow equations, a multi-period two-stage mixed-integer second-order cone programming (SOCP) robust optimization model of active and reactive coordination in distribution system with cables is developed considering the reactive power regulation capability of DG, action costs of switched capacitor reactor (SCR), on load tap changer transformer (OLTC), energy storage system (ESS), and current of shunt capacitor of cables. Further, against the deficiency of low computational rate of column and constraint generation method (CCG), a novel method iteratively solving the first and second stage model on cutting plane is proposed. In the first stage model, the number of variables and constraints keeps constant during the iteration. In the second stage model, it only needs to solve the model of each single time period. Then their results are accumulated. Thus, the computational speed using the proposed method is much higher than CCG. The effectiveness of the proposed method is separately validated on the 4-bus, IEEE 33-bus, and PG69-bus distribution systems.

Index Terms—Distribution system, robust optimization, mixed-integer second-order cone programming, cost of regulating equipment, coordinated optimization of active and reactive power

NOMENCLATURE

Indices

l	Index of nodes other than the slack node and branches whose downstream node is l.
$\mathrm{up}(l)$	The node whose downstream node is l.

Sets

$B^{\mathrm{ESS}}/B^{\mathrm{SCR}}/B^{\mathrm{DG}}$	Sets of buses with ESS/SCR/DG.
ℓ	Sets of branches.
Ψ_t	Set of discrete variables.

Parameters

$r_l/x_l/z_l/b_l$	Resistance/reactance/impedance/half shunt susceptance of branch l.
P_0/Q_0	No load active/reactive power loss of transformer.
$p_l^{\min}/p_l^{\max}$	Lower/upper bound of active power for load connected to bus l.
$q_l^{\min}/q_l^{\max}$	Lower/upper bound of reactive power for load connected to bus l.
$Q_l^{\mathrm{SVCmin}}/Q_l^{\mathrm{SVCmax}}$	Lower/upper bound of reactive power for SVC connected to bus l.
$v_{\min}/v_{\max}$	Lower/upper bound of voltage magnitude square.
$E_l^{\mathrm{ESSmin}}/E_l^{\mathrm{ESSmax}}$	Lower/upper bound of capacity for ESS connected to bus l.
$\eta_{\mathrm{ch}}/\eta_{\mathrm{dis}}$	Charge/discharge efficiency of ESS.

J. Zhang and Y. He are with the School of Electrical Engineering and Automation, Hefei University of Technology, Hefei, Anhui, 230009 China; Y. He is also with the School of Electrical Engineering, Wuhan University, Wuhan, Hubei, 430072 China.

M. Cui and F. Li are with the Department of Electrical Engineering and Computer Science, The University of Tennessee, Knoxville, TN, 37996 USA.

$P_l^{\mathrm{chmax}}/P_l^{\mathrm{dismax}}$	Upper bound of charge /discharge power for ESS connected to bus l.
c^{e}	Price for the main grid power.
c_t	Cost matrix of second stage variables.
$c^{\mathrm{ESS}}/c^{\mathrm{OLTC}}/c^{\mathrm{SCR}}$	Action price for ESS/OLTC/SCR.
Δt	Scheduling interval.
$T_{\max}$	Total number of scheduling periods.
N_{ESS}	Upper cycle limit of ESS during the scheduling periods.
$Cstep_l$	Step size of SCR connected to bus l.
$X_l^{\max}$	Upper bound of the total travel distance for SCR in a scheduling cycle.
$k^{\max}/k^{\min}$	Minimum/maximum turn ratio of OLTC.
Δk	Step size of turn ratio for OLTC.
T_t	Tap position of OLTC at time period t.
K	The highest tap position of OLTC.
$O^{\max}$	Upper bound of the total tap travel distance of OLTC in a scheduling cycle.
θ_{L}	Predicted power factor angle of load.
$\theta_l^{\min}/\theta_l^{\max}$	Minimum/maximum power factor angle of DG connected to bus l.
$I_l^{\max}$	Upper bound of current square for branch l.
$n_{\max}$	Maximum iterations.
M	A big number.
L	Length of the binary number representing the tap position.
v_0	Square of the root node voltage.
$C_l^{\min}/C_l^{\max}$	Minimum/maximum capacitance of SCR connected to bus l.
ζ	Prediction error.
ε	Convergence tolerance.
$G_{l,m}$	Adjacency matrix of the oriented graph of distribution network.

Variables

p_l/q_l	Active/reactive power load connected to bus l.
$P_l^t/Q_l^t/S_l^t$	Active/reactive/ complex power injected into the top of branch l.
$P_l^b/Q_l^b/S_l^b$	Active/reactive/complex power from the bottom of branch l.
$P_l^{\mathrm{ch}}/P_l^{\mathrm{dis}}$	Charge/discharge power for ESS at bus l.
$D_l^{\mathrm{ch}}/D_l^{\mathrm{dis}}$	Charge /discharge status for ESS at bus l.
E_l^{ESS}	Capacity for ESS connected to bus l.
$P_l^{\mathrm{DG}}/Q_l^{\mathrm{DG}}/S_l^{\mathrm{DGN}}$	Active/reactive/rated power of DG with full capacity of converter connected to bus l.
$Q_l^{\mathrm{SVC}}/Q_l^{\mathrm{SCR}}$	Reactive power of SVC/ SCR.
f_l/v_l	Current/voltage magnitude square of branch/bus l.
$\overline{S}_l^t/\overline{P}_l^t/\overline{Q}_l^t$	Upper bound of $S_l^t/P_l^t/Q_l^t$.
$\overline{S}_l^b/\overline{P}_l^b/\overline{Q}_l^b$	Upper bound of $S_l^b/P_l^b/Q_l^b$.
$\overline{v}_l/\overline{f}_l$	Upper bound of v_l/f_l.
$\hat{S}_l^t/\hat{P}_l^t/\hat{Q}_l^t$	Lower bound of $S_l^t/P_l^t/Q_l^t$.
$\hat{S}_l^b/\hat{P}_l^b/\hat{Q}_l^b$	Lower bound of $S_l^b/P_l^b/Q_l^b$.
$g_{l,t}$	Predicted active power of DG connected to bus l.
$C_{l,t}$	Capacitor of SCR.

Operators

$\Re$	Real part.
$\Im$	Imaginary part.
$*$	Conjugate operation.
$(\cdot)^{\mathrm{T}}$	Transpose of a matrix.
$\circ$	Hadamard product.

I INTRODUCTION

Electric vehicles (EVs) have great potential in reducing

fossil fuel dependence, environmental pollution, and greenhouse gas emissions. Therefore, its ownership will increase significantly in the next few years. A large number of EVs randomly connected to the power grid with uncoordinated or fast charging would aggravate the peak valley difference of load and bring about severe impacts on the economic and safe operation of distribution networks. Due to the high randomness of charging time and demand for electricity, a great challenge is brought about to the optimal control of distribution networks.

On the other hand, the penetration of renewable energy increases very rapidly. The characteristics of randomness, volatility, and anti-peak regulation of renewables bring serious threats to the real-time power balance of power grids [1]. As the problem of renewable energy consumption in distribution networks is more and more urgent, the multi-period rolling optimization can effectively solve the above problem [2].

Generally, the multi-period optimization of the active distribution network mainly consists of centralized [3, 4] and distributed [5, 6] methods. In centralized optimization, the hotspot is to relax the non-convex model to the convex programming using the radial operation structure of distribution networks [7]. The convex relaxation methods mainly include SOCP [8] and semi-definite programming (SDP) [9]. However, the SOCP model is only applicable for balanced distribution networks. Though the SDP method is applicable for unbalanced distribution networks, its computational complexity exponentially increases with the number of system nodes. Considering the development of the mixed-integer SOCP technique, it is theoretically feasible to solve the optimal power flow problem of active distribution networks with discrete variables.

In [10-12], the precision, applicability, and feasibility of SOCP relaxation for optimal power flow of distribution networks are analyzed. In [13], it is pointed out that the traditional SOCP model and its exact relaxation conditions are no longer applicable when there are coaxial cables in the distribution network since the current of shunt capacitor of coaxial cable cannot be ignored. The optimal power flow model of distribution networks is formulated considering the shunt capacitor current of cables. A set of sufficient conditions for relaxing the model to SOCP that can be checked ex-ante are developed.

The traditional deterministic optimization method may lead to voltage and current out of limit considering the uncertainty of intermittent DG and load. Robust optimization is an effective way to hedge against uncertainty [14, 15]. In [16-18], a two-stage robust optimization model is formulated and solved using the conventional CCG method.

At present, in the existing robust optimization models, the action costs of regulating equipment, reactive power regulation potential of DG, and current of shunt capacitor of cables are not considered. Further, the computational speed of CCG is very slow when the distribution system is significantly large. To cope with these, considering the action costs of ESS, SCR, and OLTC based on the branch flow equations, a two-stage multi-period mixed-integer SOCP robust optimization model is developed for active and reactive power coordination of distribution networks with cables in this paper. A fast robust optimization method iteratively solving on cutting plane is proposed. The capability of the proposed method is validated by the actual 4-bus, IEEE 33-bus, and PG69-bus distribution systems.

The organization of this paper is as follows. In Section II, the model for coordinated active and reactive optimization in a distribution network with cables is formulated. In Section III,

the two-stage mixed-integer SOCP robust optimization model is developed. In Section IV, the fast solving method is formulated. In Section V, three simulation cases are performed. Concluding remarks are summarized in Section VI.

II MODEL FOR DYNAMIC OPTIMIZATION OF ACTIVE AND REACTIVE POWER COORDINATION

2.1 Branch Flow Model of Radial Network with Cables

As shown in Fig. 1, the distribution network with a radial operation structure can be described by branch flow equations [19, 20]. Without loss of generality, we assume that only bus 1 is connected to the slack bus. When the line parameters in distribution networks meet the conditions C1~C5 in [13], the SOCP model of optimal power flow can be formulated as:

$$\min_{s,S,v,f,\hat{S},\bar{v},\bar{S},\bar{f}} \sum_{l\in\ell} \left(c\left(\Re(s_l), \Im(s_l) \right) \right) + c^{e}\left(P_1^{t} \right) \qquad (1)$$

subject to (2)~(19).

$$S_l^{t} = s_l + \sum_{m\in\ell} G_{l,m}S_m^{t} + z_l f_l - j\left(v_{\text{up}(l)} + v_l \right)b_l \qquad \forall l\in\ell \quad (2)$$

$$v_l = v_{\text{up}(l)} - 2\Re\left(z_l^{*}\left(S_l^{t} + jv_{\text{up}(l)}b_l \right) \right) + |z_l|^2 f_l \qquad \forall l\in\ell \quad (3)$$

$$f_l \geq \frac{\left| S_l^{t} + jv_{\text{up}(l)}b_l \right|^2}{v_{\text{up}(l)}} \qquad \forall l\in\ell \qquad (4)$$

$$\hat{S}_l^{t} = s_l + \sum_{m\in\ell} G_{l,m}\hat{S}_m^{t} - j\left(\bar{v}_{\text{up}(l)} + \bar{v}_l \right)b_l \qquad \forall l\in\ell \quad (5)$$

$$\bar{v}_l = \bar{v}_{\text{up}(l)} - 2\Re\left(z_l^{*}\left(\hat{S}_l^{t} + j\bar{v}_{\text{up}(l)}b_l \right) \right) \qquad \forall l\in\ell \quad (6)$$

$$\bar{S}_l^{t} = s_l + \sum_{m\in\ell} G_{l,m}\bar{S}_m^{t} + z_l\bar{f}_l - j\left(v_{\text{up}(l)} + v_l \right)b_l \qquad \forall l\in\ell \quad (7)$$

$$\bar{f}_l v_l \geq \max\left\{ \left| \hat{P}_l^{b} \right|^2, \left| \bar{P}_l^{b} \right|^2 \right\} + \max$$

$$\left\{ \left| \hat{Q}_l^{b} - \bar{v}_l b_l \right|^2, \left| \bar{Q}_l^{b} - v_l b_l \right|^2 \right\} \qquad \forall l\in\ell \qquad (8)$$

$$\bar{f}_l v_{\text{up}(l)} \geq \max\left\{ \left| \hat{P}_l^{t} \right|^2, \left| \bar{P}_l^{t} \right|^2 \right\} + \max$$

$$\left\{ \left| \hat{Q}_l^{t} + \bar{v}_{\text{up}(l)}b_l \right|^2, \left| \bar{Q}_l^{t} + v_{\text{up}(l)}b_l \right|^2 \right\} \qquad \forall l\in\ell \qquad (9)$$

$$\bar{S}_l^{b} = s_l + \sum_{m\in\ell} G_{l,m}\bar{S}_m^{t} \qquad \forall l\in\ell \qquad (10)$$

$$\hat{S}_l^{b} = s_l + \sum_{m\in\ell} G_{l,m}\hat{S}_m^{t} \qquad \forall l\in\ell \qquad (11)$$

$$v_{\min} \leq v_l \qquad \forall l\in\ell \qquad (12)$$

$$\bar{v}_l \leq v_{\max} \qquad \forall l\in\ell \qquad (13)$$

$$\left| \max\left\{ \left| \hat{P}_l^{b} \right|, \left| \bar{P}_l^{b} \right| \right\} + j\max\left\{ \left| \hat{Q}_l^{b} \right|, \left| \bar{Q}_l^{b} \right| \right\} \right|^2 \leq v_l I_l^{\max} \qquad \forall l\in\ell \quad (14)$$

$$\left| \max\left\{ \left| \hat{P}_l^{t} \right|, \left| \bar{P}_l^{t} \right| \right\} + j\max\left\{ \left| \hat{Q}_l^{t} \right|, \left| \bar{Q}_l^{t} \right| \right\} \right|^2 \leq v_{\text{up}(l)} I_l^{\max} \qquad \forall l\in\ell \quad (15)$$

$$P_l^{t} \leq \bar{P}_l^{t} \qquad \forall l\in\ell \qquad (16)$$

$$Q_l^{t} \leq \bar{Q}_l^{t} \qquad \forall l\in\ell \qquad (17)$$

$$p_l^{\min} \leq \Re(s_l) \leq p_l^{\max} \qquad \forall l\in\ell \qquad (18)$$

$$q_l^{\min} \leq \Im(s_l) \leq q_l^{\max} \qquad \forall l\in\ell \qquad (19)$$

Considering the regulating equipment, DG, and multiple time period t, Eq. (2) can be formulated as:

$$P_{l,t}^{t} = p_{l,t} - P_{l,t}^{DG} - P_{l,t}^{ESS} + \sum_{m\in\ell} G_{l,m}P_{m,t}^{t} + r_l f_{l,t} \qquad \forall l\in\ell \quad (20)$$

$$Q_{l,t}^{t} = q_{l,t} - Q_{l,t}^{DG} - Q_{l,t}^{SVC} - Q_{l,t}^{SCR} + \sum_{m\in\ell} G_{l,m}Q_{m,t}^{t}$$

$$+ x_l f_{l,t} - \left(v_{\text{up}(l),t} + v_{l,t} \right)b_l \qquad \forall l\in\ell \qquad (21)$$

Eq. (3) can be formulated as:

$$v_{l,t} = v_{\mathrm{up}(l),t} - 2r_l P_{l,t}^{\mathrm{t}} - 2x_l\left(Q_{l,t}^{\mathrm{t}} + v_{\mathrm{up}(l),t}b_l\right) \\ + |z_l|^2 f_{l,t} \quad \forall l \in \ell \tag{22}$$

Eq. (4) can be formulated as:

$$f_{l,t}v_{\mathrm{up}(l),t} \geq \left|P_{l,t}^{\mathrm{t}}\right|^2 + \left|Q_{l,t}^{\mathrm{t}} + v_{\mathrm{up}(l),t}b_l\right|^2 \quad \forall l \in \ell \tag{23}$$

Eq. (5) can be formulated as:

$$\hat{P}_{l,t}^{\mathrm{t}} = p_{l,t} - P_{l,t}^{\mathrm{DG}} - P_{l,t}^{\mathrm{ESS}} + \sum_{m\in\ell} G_{l,m}\hat{P}_{m,t}^{\mathrm{t}} \quad \forall l \in \ell \tag{24}$$

$$\hat{Q}_{l,t}^{\mathrm{t}} = q_{l,t} - Q_{l,t}^{\mathrm{DG}} - Q_{l,t}^{\mathrm{SVC}} - Q_{l,t}^{\mathrm{SCR}} + \\ \sum_{m\in\ell} G_{l,m}\hat{Q}_{m,t}^{\mathrm{t}} - \left(\overline{v}_{\mathrm{up}(l),t} + \overline{v}_{l,t}\right)b_l \quad \forall l \in \ell \tag{25}$$

Eq. (6) can be formulated as:

$$\overline{v}_l = \overline{v}_{\mathrm{up}(l)} - 2r_l\hat{P}_{l,t}^{\mathrm{t}} - 2x_l\left(\hat{Q}_{l,t}^{\mathrm{t}} + \overline{v}_{\mathrm{up}(l),t}b_l\right) \quad \forall l \in \ell \tag{26}$$

Eq. (7) can be formulated as:

$$\overline{P}_{l,t}^{\mathrm{t}} = p_{l,t} - P_{l,t}^{\mathrm{DG}} - P_{l,t}^{\mathrm{ESS}} + \sum_{m\in\ell} G_{l,m}\overline{P}_{m,t}^{\mathrm{t}} + r_l\overline{f}_{l,t} \quad \forall l \in \ell \tag{27}$$

$$\overline{Q}_{l,t}^{\mathrm{t}} = q_{l,t} - Q_{l,t}^{\mathrm{DG}} - Q_{l,t}^{\mathrm{SVC}} - Q_{l,t}^{\mathrm{SCR}} + \sum_{m\in\ell} G_{l,m}\overline{Q}_{m,t}^{\mathrm{t}} \\ + x_l\overline{f}_{l,t} - \left(v_{\mathrm{up}(l),t} + v_{l,t}\right)b_l \quad \forall l \in \ell \tag{28}$$

Eq. (8) can be formulated as:

$$\begin{cases} \overline{f}_{l,t}v_{l,t} \geq \left|\hat{P}_{l,t}^{\mathrm{b}}\right|^2 + \left|\hat{Q}_{l,t}^{\mathrm{b}} - \overline{v}_{l,t}b_l\right|^2 \\ \overline{f}_{l,t}v_{l,t} \geq \left|\hat{P}_{l,t}^{\mathrm{b}}\right|^2 + \left|\overline{Q}_{l,t}^{\mathrm{b}} - v_{l,t}b_l\right|^2 \\ \overline{f}_{l,t}v_{l,t} \geq \left|\overline{P}_{l,t}^{\mathrm{b}}\right|^2 + \left|\hat{Q}_{l,t}^{\mathrm{b}} - \overline{v}_{l,t}b_l\right|^2 \\ \overline{f}_{l,t}v_{l,t} \geq \left|\overline{P}_{l,t}^{\mathrm{b}}\right|^2 + \left|\overline{Q}_{l,t}^{\mathrm{b}} - v_{l,t}b_l\right|^2 \end{cases} \quad \forall l \in \ell \tag{29}$$

Eq. (9) can be formulated as:

$$\begin{cases} \overline{f}_{l,t}v_{\mathrm{up}(l),t} \geq \left|\hat{P}_{l,t}^{\mathrm{t}}\right|^2 + \left|\hat{Q}_{l,t}^{\mathrm{t}} + \overline{v}_{\mathrm{up}(l),t}b_l\right|^2 \\ \overline{f}_{l,t}v_{\mathrm{up}(l),t} \geq \left|\hat{P}_{l,t}^{\mathrm{t}}\right|^2 + \left|\overline{Q}_{l,t}^{\mathrm{t}} + v_{\mathrm{up}(l),t}b_l\right|^2 \\ \overline{f}_{l,t}v_{\mathrm{up}(l),t} \geq \left|\overline{P}_{l,t}^{\mathrm{t}}\right|^2 + \left|\hat{Q}_{l,t}^{\mathrm{t}} + \overline{v}_{\mathrm{up}(l),t}b_l\right|^2 \\ \overline{f}_{l,t}v_{\mathrm{up}(l),t} \geq \left|\overline{P}_{l,t}^{\mathrm{t}}\right|^2 + \left|\overline{Q}_{l,t}^{\mathrm{t}} + v_{\mathrm{up}(l),t}b_l\right|^2 \end{cases} \quad \forall l \in \ell \tag{30}$$

Eq. (10) can be formulated as:

$$\overline{P}_{l,t}^{\mathrm{b}} = p_{l,t} - P_{l,t}^{\mathrm{DG}} - P_{l,t}^{\mathrm{ESS}} + \sum_{m\in\ell} G_{l,m}\overline{P}_{m,t}^{\mathrm{t}} \quad \forall l \in \ell \tag{31}$$

$$\overline{Q}_{l,t}^{\mathrm{b}} = q_{l,t} - Q_{l,t}^{\mathrm{DG}} - Q_{l,t}^{\mathrm{SVC}} - Q_{l,t}^{\mathrm{SCR}} + \sum_{m\in\ell} G_{l,m}\overline{Q}_{m,t}^{\mathrm{t}} \quad \forall l \in \ell \tag{32}$$

Eq. (11) can be formulated as:

$$\hat{P}_{l,t}^{\mathrm{b}} = p_{l,t} - P_{l,t}^{\mathrm{DG}} - P_{l,t}^{\mathrm{ESS}} + \sum_{m\in\ell} G_{l,m}\hat{P}_{m,t}^{\mathrm{t}} \quad \forall l \in \ell \tag{33}$$

$$\hat{Q}_{l,t}^{\mathrm{b}} = q_{l,t} - Q_{l,t}^{\mathrm{DG}} - Q_{l,t}^{\mathrm{SVC}} - Q_{l,t}^{\mathrm{SCR}} + \sum_{m\in\ell} G_{l,m}\hat{Q}_{m,t}^{\mathrm{t}} \quad \forall l \in \ell \tag{34}$$

Eq. (14) can be formulated as:

$$\begin{cases} v_{l,t}I_l^{\max} \geq \left|\hat{P}_{l,t}^{\mathrm{b}}\right|^2 + \left|\hat{Q}_{l,t}^{\mathrm{b}}\right|^2 \\ v_{l,t}I_l^{\max} \geq \left|\hat{P}_{l,t}^{\mathrm{b}}\right|^2 + \left|\overline{Q}_{l,t}^{\mathrm{b}}\right|^2 \\ v_{l,t}I_l^{\max} \geq \left|\overline{P}_{l,t}^{\mathrm{b}}\right|^2 + \left|\hat{Q}_{l,t}^{\mathrm{b}}\right|^2 \\ v_{l,t}I_l^{\max} \geq \left|\overline{P}_{l,t}^{\mathrm{b}}\right|^2 + \left|\overline{Q}_{l,t}^{\mathrm{b}}\right|^2 \end{cases} \quad \forall l \in \ell \tag{35}$$

Eq. (15) can be converted into:

$$\begin{cases} v_{\mathrm{up}(l),t}I_l^{\max} \geq \left|\hat{P}_{l,t}^{\mathrm{t}}\right|^2 + \left|\hat{Q}_{l,t}^{\mathrm{t}}\right|^2 \\ v_{\mathrm{up}(l),t}I_l^{\max} \geq \left|\hat{P}_{l,t}^{\mathrm{t}}\right|^2 + \left|\overline{Q}_{l,t}^{\mathrm{t}}\right|^2 \\ v_{\mathrm{up}(l),t}I_l^{\max} \geq \left|\overline{P}_{l,t}^{\mathrm{t}}\right|^2 + \left|\hat{Q}_{l,t}^{\mathrm{t}}\right|^2 \\ v_{\mathrm{up}(l),t}I_l^{\max} \geq \left|\overline{P}_{l,t}^{\mathrm{t}}\right|^2 + \left|\overline{Q}_{l,t}^{\mathrm{t}}\right|^2 \end{cases} \quad \forall l \in \ell \tag{36}$$
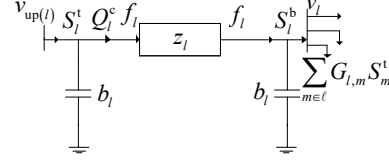

Fig. 1. Radial distribution system with cables.

2.2 Model of ESS

1) Power constraints

$$P_{l,t}^{\mathrm{ESS}} = P_{l,t}^{\mathrm{dis}} - P_{l,t}^{\mathrm{ch}} \tag{37}$$

$$0 \leq P_{l,t}^{\mathrm{dis}} \leq P_l^{\mathrm{dismax}} D_{l,t}^{\mathrm{dis}} \tag{38}$$

$$0 \leq P_{l,t}^{\mathrm{ch}} \leq P_l^{\mathrm{chmax}} D_{l,t}^{\mathrm{ch}} \tag{39}$$

2) Capacity constraints

$$E_{l,t}^{\mathrm{ESS}} + \eta_{\mathrm{ch}} P_{l,t}^{\mathrm{ch}}\Delta t - \frac{P_{l,t}^{\mathrm{dis}}}{\eta_{\mathrm{dis}}}\Delta t = E_{l,t+1}^{\mathrm{ESS}}, t = 1,2,\cdots T_{\max}-1 \tag{40}$$

$$E_{l,t}^{\mathrm{ESS}} + \eta_{\mathrm{ch}} P_{l,t}^{\mathrm{ch}}\Delta t - \frac{P_{l,t}^{\mathrm{dis}}}{\eta_{\mathrm{dis}}}\Delta t = E_{l,1}^{\mathrm{ESS}}, t = T_{\max} \tag{41}$$

$$E_l^{\mathrm{ESSmin}} \leq E_{l,t}^{\mathrm{ESS}} \leq E_l^{\mathrm{ESSmax}} \tag{42}$$

3) Charge and discharge state constraint

$$D_{l,t}^{\mathrm{ch}} + D_{l,t}^{\mathrm{dis}} \leq 1 \tag{43}$$

$$D_{l,t}^{\mathrm{ch}} \in \{0,1\} \tag{44}$$

$$D_{l,t}^{\mathrm{dis}} \in \{0,1\} \tag{45}$$

4) Cycle limit of charge and discharge

$$\sum_{t=1}^{T_{\max}} \eta_{\mathrm{ch}} P_{l,t}^{\mathrm{ch}}\Delta t \leq N_{\mathrm{ESS}} E_l^{\mathrm{ESS}} \tag{46}$$

5) Cost of ESS

$$C_l^{\mathrm{ESS}} = \sum_{t=1}^{T_{\max}}\Delta t\left(c_l^{\mathrm{ESS}}\left(P_{l,t}^{\mathrm{ch}} + P_{l,t}^{\mathrm{dis}}\right) + c^{\mathrm{e}}\left(1-\eta_{\mathrm{ch}}\right)P_{l,t}^{\mathrm{ch}} + c^{\mathrm{e}}\left(\frac{1}{\eta_{\mathrm{dis}}}-1\right)P_{l,t}^{\mathrm{dis}}\right) \tag{47}$$

2.3 Model of SVC

$$Q_l^{\mathrm{SVC\,min}} \leq Q_{l,t}^{\mathrm{SVC}} \leq Q_l^{\mathrm{SVC\,max}} \tag{48}$$

2.4 Model of SCR

1) Linearization of injected reactive power from SCR

The reactive power injected into the grid from SCR connected to node l at time period t is:

$$Q_{l,t}^{\mathrm{SCR}} = v_{l,t}C_{l,t} \tag{49}$$

Eq. (49) can be linearized as follows. The total number of SCR groups is $\frac{C_l^{\max} - C_l^{\min}}{Cstep_l}+1$. Let u_l+1 be the length of the binary number that is used to represent the number of SCR groups put into operation. The integer u_l can be determined according to:

$$\log_2\left(\frac{C_l^{\max} - C_l^{\min}}{Cstep_l}+1\right)-1 < u_l \leq \log_2\left(\frac{C_l^{\max} - C_l^{\min}}{Cstep_l}+1\right) \tag{50}$$

Then the capacitor of SCR put into operation can be expressed as:

$$C_{l,t} = C_l^{\min} + Cstep_l\left(2^0 w_{l0,t} + 2^1 w_{l1,t} + \cdots 2^{u_l} w_{lu_l,t}\right) \quad (51)$$

$$2^0 w_{l0,t} + 2^1 w_{l1,t} + \cdots 2^{u_l} w_{lu_l,t} \leq \frac{C_l^{\max} - C_l^{\min}}{Cstep_l} \quad (52)$$

$$w_{l0,t}, w_{l1,t}, \cdots w_{lu_l,t} \in \{0,1\} \quad (53)$$

The reactive power injected from SCR can be expressed as:

$$Q_{l,t}^{\text{SCR}} = C_l^{\min} v_{l,t} + Cstep_l\left(2^0 w_{l0,t} v_{l,t} + 2^1 w_{l1,t} v_{l,t} + \cdots 2^{u_l} w_{lu_l,t} v_{l,t}\right) \quad (54)$$

By introducing dummy variables $\sigma_{l0,t}$, $\sigma_{l1,t}$, …, and $\sigma_{lu_l,t}$, Eq. (54) can be linearized using the big M method, given by:

$$Q_{l,t}^{\text{SCR}} = C_l^{\min} v_{l,t} + Cstep_l\left(2^0 \sigma_{l0,t} + 2^1 \sigma_{l1,t} + \cdots 2^{u_l} \sigma_{lu_l,t}\right) \quad (55)$$

$$0 \leq v_{l,t} - \sigma_{lk,t} \leq M\left(1 - w_{lk,t}\right) \quad (56)$$

$$0 \leq \sigma_{lk,t} \leq M w_{lk,t} \quad (57)$$

2) Linearization of SCR travel distance constraint

Between time periods t and $t+1$, the number of change for SCR groups put into operation is:

$$X_{l,t} = \left|\sum_{n=0}^{u_l} 2^n w_{ln,t+1} - \sum_{n=0}^{u_l} 2^n w_{ln,t}\right|, t = 1,2,\cdots T_{\max} - 1 \quad (58)$$

The absolute value sign $|\cdot|$ in (58) can be removed by introducing a binary dummy variable $\rho_{l,t}$. Thus, Eq. (58) can be expressed as:

$$X_{l,t} \geq 0 \quad (59)$$

$$X_{l,t} = \sum_{n=0}^{u_l} 2^n (\varpi_{ln,t+1} - \varpi_{ln,t})(2\rho_{l,t} - 1) \quad (60)$$

$$= -\sum_{n=0}^{u_l} 2^n (\varpi_{ln,t+1} - \varpi_{ln,t}) + \sum_{n=0}^{u_l} 2^{n+1}(\varpi_{ln,t+1} - \varpi_{ln,t})\rho_{l,t}$$

$$\rho_{l,t} \in \{0,1\} \quad (61)$$

Define $\chi_{l,t} = \sum_{n=0}^{u_l} 2^{n+1}(\varpi_{ln,t+1} - \varpi_{ln,t})\rho_{l,t}$. Eq. (60) can be linearized using the big M method, given by:

$$X_{l,t} = -\sum_{n=0}^{u_l} 2^n (\varpi_{ln,t+1} - \varpi_{ln,t}) + \chi_{l,t} \quad (62)$$

$$0 \leq \chi_{l,t} \leq \rho_{l,t} M \quad (63)$$

$$-(1-\rho_{l,t})M \leq \sum_{n=0}^{u_l} 2^{n+1}(\varpi_{ln,t+1} - \varpi_{ln,t}) - \chi_{l,t} \leq (1-\rho_{l,t})M \quad (64)$$

The travel distance constraint in a scheduling cycle is:

$$\sum_{t=1}^{T_{\max}-1} X_{l,t} \leq X_l^{\max} \quad (65)$$

3) Action cost of SCR

$$C_l^{\text{SCR}} = c_l^{\text{SCR}} \sum_{t=1}^{T_{\max}-1} X_{l,t} \quad (66)$$

2.5 Model of OLTC

1) Linearization of turn ratio square for OLTC

The model of OLTC is shown in Fig. 2. The turn ratio of OLTC connected to the root node can be expressed as:

$$k_t = k^{\min} + T_t \Delta k \quad (67)$$

$$K = \left(k^{\max} - k^{\min}\right) / \Delta k \quad (68)$$

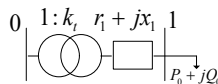$$0 \leq T_t \leq K \quad (69)$$

Fig. 2. Schematic diagram of OLTC.

Let T_t be represented by binary numbers. Then Eqs. (67)-(69) can be expressed as:

$$k_t = k^{\min} + \Delta k \sum_{n=0}^{L} 2^n \beta_{n,t} \quad (70)$$

$$\sum_{n=0}^{L} 2^n \beta_{n,t} \leq K \quad (71)$$

$$\beta_{n,t} \in \{0,1\} \quad (72)$$

The square of the secondary side voltage for OLTC can be expressed as:

$$v_{\text{Tr},t} = v_0(k_t k^{\min} + \Delta k \sum_{n=0}^{L} 2^n k_t \beta_{n,t}) \quad (73)$$

Define $Y_{n,t} = k_t \beta_{n,t}$. Then Eq. (73) can be expressed as:

$$v_{\text{Tr},t} = v_0\left(k_t k^{\min} + \Delta k \sum_{n=0}^{L} 2^n Y_{n,t}\right) \quad (74)$$

$$0 \leq k_t - Y_{n,t} \leq M\left(1 - \beta_{n,t}\right) \quad (75)$$

$$0 \leq Y_{n,t} \leq M \beta_{n,t} \quad (76)$$

2) Linearization of travel distance constraints for OLTC

The tap position difference of OLTC between time periods t and $t+1$ is formulated as:

$$O_t = \left|\sum_{n=0}^{L} 2^n \beta_{n,t} - \sum_{n=0}^{L} 2^n \beta_{n,t}\right|, t = 1,2,\cdots T_{\max} - 1 \quad (77)$$

The sign of absolute value can be removed by introducing a dummy variable μ_t. Eq. (77) can be expressed as:

$$O_t \geq 0 \quad (78)$$

$$O_t = \sum_{n=0}^{L} 2^n (\beta_{n,t+1} - \beta_{n,t})(2\mu_t - 1) \quad (79)$$

$$= -\sum_{n=0}^{L} 2^n (\beta_{n,t+1} - \beta_{n,t}) + \sum_{n=0}^{L} 2^{n+1}(\beta_{n,t+1} - \beta_{n,t})\mu_t$$

$$\mu_t \in \{0,1\} \quad (80)$$

Define $\alpha_t = \sum_{n=0}^{L} 2^{n+1}(\beta_{n,t+1} - \beta_{n,t})\mu_t$. Then Eq. (79) can be expressed as:

$$O_t = -\sum_{n=0}^{L} 2^n (\beta_{n,t+1} - \beta_{n,t}) + \mu_t \quad (81)$$

$$0 \leq \alpha_t \leq \mu_t M \quad (82)$$

$$-\left(1-\mu_t\right)M \leq \sum_{n=0}^{L} 2^{n+1}\left(\beta_{n,t+1} - \beta_{n,t}\right) - \alpha_t \leq \left(1-\mu_t\right)M \quad (83)$$

The total travel distance constraint of tap in a scheduling cycle is:

$$\sum_{t=1}^{T_{\max}-1} O_t \leq O^{\max} \quad (84)$$

3) Action cost of OLTC

$$C^{\text{OLTC}} = c^{\text{OLTC}} \sum_{t=1}^{T_{\max}-1} O_t \quad (85)$$

2.6 Model of DG

1) Constraint on power factor

$$P_{l,t}^{\text{DG}} \tan\left(\theta_l^{\min}\right) \leq Q_{l,t}^{\text{DG}} \leq P_{l,t}^{\text{DG}} \tan\left(\theta_l^{\max}\right) \quad (86)$$

2) Constraint on active power

$$0 \leq P_{l,t}^{\text{DG}} \leq g_{l,t} \quad (87)$$

3) Constraint on capacity

$$\sqrt{\left(P_{l,t}^{\text{DG}}\right)^2 + \left(Q_{l,t}^{\text{DG}}\right)^2} \leq S_l^{\text{DGN}} \quad (88)$$

2.7 Objective Function

The objective function is to minimize the total costs:

$$f_{\text{obj}} = \min\left(\sum_{t=1}^{T_{\max}}\left(c^{\text{e}}P_{1,t}^{\text{t}}\Delta t\right) + \sum_{l \in B^{\text{ESS}}} C_l^{\text{ESS}} + C^{\text{OLTC}} + \sum_{l \in B^{\text{SCR}}} C_l^{\text{SCR}}\right) \quad (89)$$

III MODEL OF ROBUST OPTIMIZATION

3.1 Model of Deterministic Optimization

A two-stage optimization method is adopted in this paper. The discrete variables associated with OLTC, SCR, and variables associated with ESS are the first-stage variables. The first stage variables denoted as $\{\psi_t\}$ cannot be adjusted after the uncertainties are revealed. They are regarded as the "here and after" decisions. The continuous variables, such as the reactive power of SVC, branch power, current, node voltage, etc., are the second-stage variables. The second-stage variables denoted as $\{\varphi_t\}$ can be flexibly adjusted in the real-time operation when the uncertainties are revealed. They are regarded as the "wait and see" decisions.

For clear presentation, the deterministic optimization model can be written in a compact form as:

$$\text{MP:} \quad f_{\text{mp}} = \min_{\{\psi_t\},\{\varphi_t\}} f_{\text{obj}} \quad (90a)$$

$$\text{s.t.} \quad \psi_t \in \Psi_t \quad (90b)$$

$$\sum_{t=1}^{T_{\max}} A_t^T \psi_t \leq b \quad (90c)$$

$$B_t^T \psi_t \leq b_{1t} \quad (90d)$$

$$J_t \varphi_t \leq b_{2t} \quad (90e)$$

$$L_t \psi_t + N_t \varphi_t \leq b_{3t} \quad (90f)$$

$$D_{i,t}^{\text{p}} \psi_t + E_{i,t}^{\text{p}} \varphi_t = d_t^{\text{p}} \quad i = 1,2,3,4,5 \quad (90g)$$

$$D_{i,t}^{\text{q}} \psi_t + E_{i,t}^{\text{q}} \varphi_t = d_t^{\text{q}} \quad i = 1,2,3,4,5 \quad (90h)$$

$$H_{l,t} \varphi_t \leq g_{l,t} \quad \forall l \in B^{\text{DG}} \quad (90i)$$

$$\|K_{nt} \varphi_t\| \leq h_{nt}^T \varphi_t \quad (90j)$$

Eq. (90a) indicates the total cost minimization. Eq. (90b) represents the feasible set of the first stage variables. Eq. (90c) represents the coupling relationship of the first-stage variables between different time periods. Eq. (90d) represents the inequality for first stage variables at each time period. Eq. (90e) summarizes the inequality of the second-stage variables at each time period. Eq. (90f) denotes the relationship between the first and second stage variables at each time period. Eqs. (90g) and (90h) represent the active and reactive power flow constraint at each time period corresponding to (2), (5), (7), (10), and (11). Eq. (90i) represents the constraints on the active power of DG. Eq. (90j) represents all second-order cone constraints associated with all branches and DG.

3.2 Model of Robust Optimization

Since intermittent DG and load have strong randomness, it is challenging to avoid voltage or current exceeding limits if the deterministic optimization model is adopted. Thus, a robust optimization model is constructed as:

$$\min_{\{\psi_t\}} \max_{\substack{d_t \in D_t \\ g_t \in G_t}} \min_{\{\varphi_t\}} f_{\text{obj}} \quad (91a)$$

$$\text{s.t. (90b)}\sim(90j)$$

$$D_t = \left\{\left(d_t^{\text{p}}, d_t^{\text{q}}\right) \middle| d_t^{\min} \leq d_t^{\text{p}} \leq d_t^{\max}, d_t^{\min} \circ \tan\left(\theta_{\text{L}}\right) \leq d_t^{\text{q}} \leq d_t^{\max} \circ \tan\left(\theta_{\text{L}}\right)\right\} \quad (91b)$$

$$G_t = \left\{g_{l,t} \middle| g_{l,t}^{\min} \leq g_{l,t} \leq g_{l,t}^{\max}\right\} \quad \forall l \in B^{\text{DG}} \quad (91c)$$

The physical meaning of (91) is that the first-stage solution

minimizes the total costs in the worst scenario. The inner max-min model seeks to find out the worst scenario.

IV SOLVING METHOD OF ROBUST OPTIMIZATION MODEL

4.1 Master and Sub-Problem

The master problem is shown in (90a)~(90j). The objective of the master problem is to find the optimal values of the first-stage variables given the scenario generated by the sub-problem. It gives a lower bound of the original problem (91). The optimal values of the first-stage variables, such as capacitance of SCR, turn ratios of OLTC, and injected power of ESS, are substituted into the power flow equations in (2), (5), (7), (10), and (11). Thus, the model of the sub-problem is formulated as below:

$$\text{SP:} \quad L\left(\psi_1^*, \cdots \psi_{T_{\max}}^*\right) = \max_{\substack{d_t \in D_t \\ g_t \in G_t}} \min \sum_{t=1}^{T_{\max}}\left(c_t^T y_t\right) \quad (92a)$$

$$R_t y_t = b_{1t} \,\forall t, \left(\pi_{1t}\right) \quad (92b)$$

$$M_t y_t \leq b_{2t} \,\forall t, \left(\pi_{2t}\right) \quad (92c)$$

$$W_{i,t}^{\text{p}} \varphi_t = d_t^{\text{p}} + d_{0t}^{\text{p}} \quad i = 1,2,3,4,5 \quad \forall t, \left(\pi_{3t}^{(i)}\right) \quad (92d)$$

$$W_{i,t}^{\text{q}} \varphi_t = d_t^{\text{q}} \quad i = 1,2,3,4,5 \quad \forall t, \left(\pi_{4t}^{(i)}\right) \quad (92e)$$

$$I_{l,t} y_t \leq g_{l,t} \quad \forall l \in B^{\text{DG}} \; \forall t, \left(\pi_{5t}^{(l)}\right) \quad (92f)$$

$$\|K_{nt} y_t\| \leq h_{nt}^T y_t \quad \forall t, \left(\pi_{6nt}, \pi_{7nt}\right) \quad (92g)$$

It is worth noting that y_t is different from φ_t. This is because only continuous variables such as branch power, current, node voltage, and SVC reactive power are included in y_t. However, some auxiliary variables that are used to linearize nonlinear equations such as $\sigma_{lk,t}$ are also included in φ_t.

The max-min bi-level optimization of (92a)~(92g) can be transformed into the following single-level optimization using the dual theory.

$$\text{SP:} \quad \sum_{t=1}^{T_{\max}} \max_{d_t, g_t, \pi_{1t}, \pi_{2t}, \pi_{3t}, \pi_{4t}, \pi_{5t}, \pi_{6nt}, \pi_{7nt}} \left(b_{1t}^{\text{T}}\pi_{1t} + b_{2t}^{\text{T}}\pi_{2t} + \left(d_t^{\text{p}} + d_{0t}^{\text{p}}\right)^{\text{T}}\sum_{i=1}^{5}\pi_{3t}^{(i)} + \left(d_t^{\text{q}}\right)^{\text{T}}\sum_{i=1}^{5}\pi_{4t}^{(i)} + \sum_{l \in B^{\text{DG}}} g_{l,t}\pi_{5t}^{(l)}\right) \quad (93a)$$

$$\text{s.t.} \quad \|\pi_{6nt}\| \leq \pi_{7nt}, \forall t \quad (93b)$$

$$R_t^{\text{T}}\pi_{1t} + M_t^{\text{T}}\pi_{2t} + \sum_{i=1}^{5}\left(W_{i,t}^{\text{p}}\right)^{\text{T}}\pi_{3t}^{(i)} + \sum_{i=1}^{5}\left(W_{i,t}^{\text{q}}\right)^{\text{T}}\pi_{4t}^{(i)} + \sum_{k=1}^{n_0}\left(I_{k,t}\right)^{\text{T}}\pi_{5t}^{(i)} + \sum_n\left(K_{nt}^{\text{T}}\pi_{6nt} + h_{nt}\pi_{7nt}\right) = c_t, \forall t \quad (93c)$$

$$\pi_{2t} \leq 0, \forall t \quad (93d)$$

$$d_t^{\min} \leq d_t^{\text{p}} \leq d_t^{\max}, \forall t \quad (93e)$$

$$d_t^{\min} \circ \tan\left(\theta_{\text{L}}\right) \leq d_t^{\text{q}} \leq d_t^{\max} \circ \tan\left(\theta_{\text{L}}\right), \forall t \quad (93f)$$

$$g_{l,t}^{\min} \leq g_{l,t} \leq g_{l,t}^{\max}, \forall t, \quad \forall l \in B^{\text{DG}} \quad (93g)$$

It can be seen from (93a)~(93g) that the constraints of each time period are independent of each other. Moreover, the objective function is cumulative with respect to each time period. The sub-problem only needs to be solved and then accumulated for each time period. As a consequence, the computational rate is significantly enhanced.

Let $\pi_{3t} = \sum_{i=1}^{5}\pi_{3t}^{(i)}$, $\gamma_{t,n}^{\text{p}} = \pi_{3t}\delta_{t,n}$, then $\left(d_t^{\text{p}}\right)^{\text{T}}\pi_{3t}$ can be linearized as:

$$\begin{cases} \left(d_t^p\right)^T \pi_{3t} = \sum_n \left(d_{t,n}^{pmin}\pi_{3t,n} + \left(d_{t,n}^{pmax} - d_{t,n}^{pmin}\right)\gamma_{t,n}^p\right) \\ -M\delta_{t,n} \le \gamma_{t,n}^p \le M\delta_{t,n} \\ -M\left(1-\delta_{t,n}\right) \le \gamma_{t,n}^p - \pi_{3t,n} \le M\left(1-\delta_{t,n}\right) \\ \delta_{t,n} \in \{0,1\} \end{cases} \quad \forall t, \forall n \quad (94a)$$

Similarly, let $\pi_{4t} = \sum_{i=1}^5 \pi_{4t}^{(i)}$, $\gamma_{t,n}^q = \pi_{4t}\delta_{t,n}$, then $\left(d_t^q\right)^T \pi_{4t}$ can be linearized as:

$$\begin{cases} \left(d_t^q\right)^T \pi_{4t} = \sum_n \left(d_{t,n}^{pmin}\tan\left(\theta_{L,n}\right)\pi_{4t,n} + \left(d_{t,n}^{pmax} - d_{t,n}^{pmin}\right)\tan\left(\theta_{L,n}\right)\gamma_{t,n}^q\right) \\ -M\delta_{t,n} \le \gamma_{t,n}^q \le M\delta_{t,n} \\ -M\left(1-\delta_{t,n}\right) \le \gamma_{t,n}^q - \pi_{4t,n} \le M\left(1-\delta_{t,n}\right) \end{cases} \quad \forall t, \forall n \quad (94b)$$

Similarly, let $\gamma_{l,t}^{DG} = \lambda_t \pi_{5t}^{(l)}$, for the same kind of renewable DG, such as wind turbine, $g_{l,t}\pi_{5t}^{(l)}$ can be linearized as:

$$\begin{cases} g_{l,t}\pi_{5t}^{(l)} = \left(g_{l,t}^{min}\pi_{5t}^{(l)} + \left(g_{l,t}^{max} - g_{l,t}^{min}\right)\gamma_{l,t}^{DG}\right) \\ -M\lambda_t \le \gamma_{l,t}^{DG} \le M\lambda_t \\ -M\left(1-\lambda_t\right) \le \gamma_{l,t}^{DG} - \pi_{5t}^{(l)} \le M\left(1-\lambda_t\right) \\ \lambda_t \in \{0,1\} \end{cases} \quad \forall t, \forall l \in B^{DG} \quad (94c)$$

4.2 Solving Steps

The two-stage fast robust optimization method proposed in this paper does not need to increase variables and constraints. The solving steps are as follows.

P1: Set $LB = -\infty$, $UB = +\infty$, and $n = 1$.

P2: Given a scenario, solve MP to obtain the optimal solution $\left(\psi_t^*, \varphi_t^*, f_{mp}^*\right)$. Compute $f_\varphi^* = \sum_{t=1}^{T_{max}}\left(c^e P_{1,t}^t \Delta t\right)$ and update lower bound to $LB = f_\varphi^*$.

P3: Fix $\{\psi_t^*\}$ and solve the SP at each time period to obtain the worst scenario $\{d_t^*\}$, $\{g_t^*\}$. Then the optimal objective function value of each time period is accumulated to obtain the total optimal objective function $f_{sp}^*\left(\psi_t^*\right)$.

P4: Update upper bound to $UB = f_{sp}^*\left(\psi_t^*\right)$. If $|LB - UB| < \varepsilon$ or $n > n_{max}$ (n_{max} is the maximum number of iterations), the program is terminated and ψ_t^* is output. Otherwise, $\{d_t^*\}$ and $\{g_t^*\}$ are substituted into MP.

P5: Update $n = n+1$ and go to P2.

V NUMERICAL ANALYSIS

5.1 Configuration of Three Test Systems

Three radial distribution systems are adopted to test the capability of the proposed method including a 4-bus, IEEE 33-bus, and PG69-bus distribution networks with uncertain wind power generation and load. The topology of the 4-bus distribution system is shown in Fig. 3, while topologies of the IEEE 33-bus and PG69-bus distribution systems are shown in Appendix A and B [21]. All the programs are developed in MATLAB R2018a. The mixed-integer SOCP toolbox of MOSEK 9.1.4 is used to solve the mater and sub-problem. The hardware of the computer is Intel XEON i5-E5640 with 2.67 GHz CPU and 32 GB memory. To save memory, the sparse matrix is compressed and stored.

The parameters of the 4-bus distribution system are the same as those in Table I of [13] except that the length of both cables is 20 km. The shunt capacitor of each cable for the IEEE-33 and PG69-bus distribution systems is shown in Appendix C and D [21], respectively.

The base power of the three systems is chosen to be 5, 10, and 10 MVA, respectively. The base voltage of the three systems is chosen to be 24.9, 12.66, and 12.66 kV, respectively. There is one OLTC transformer connected to the root node for the three systems. The impedance of the transformer is $0.02 + j0.105$ p.u. The minimum and maximum turn ratios of OLTC are 0.94 and 1.06, respectively. The step size of the turn ratio is 0.01. The voltage bound on each bus is [0.9, 1.1]. The root node is taken as the slack node whose voltage is fixed to 1.0 p.u. The current limit at each branch is 120 A for the 4-bus system, and 400 A for the IEEE-33 and PG69-bus distribution systems, respectively. The big M is set to be 100. Convergence tolerance ε is set to be 0.0001. The maximum iteration is set to be 7. The optimization period is 0:00~24:00 and the interval is 1 hour.

There are one SCR connected to node 1 for the 4-bus system, one SCR connected to nodes 3 and 6 for the 33-bus system, and one SCR connected to node 19, 36, 41, 53, and 64 for the 69-bus system, respectively. All the capacity of SCR is [-0.3 0.3], [-0.6 0.6], and [-0.6 0.6] Mvar, while the step size is 0.05, 0.1, and 0.1 Mvar for three systems, respectively. The maximum travel distance of OLTC and SCR is 24.

There are one SVC connected to node 3 for the 4-bus system, one SVC connected to node 18 for the 33-bus system, and one SVC connected to node 3 and 11 for the 69-bus system, respectively. The capacity of SVC in the three distribution networks is [-0.15 0.15], [-0.5 0.5], and [-0.5 0.5] Mvar, respectively.

There are one permanent magnet direct drive wind turbine (PMSG) connected to node 3 for the 4-bus system, one PMSG connected to node 13, 21, 24, and 31 for the 33-bus system, and one PMSG connected to node 19, 41, 54, 56, and 66 for the 69-bus system, respectively. The capacity of each PMSG in the three distribution networks is 5, 0.4, and 0.3 MVA, respectively.

There are one ESS connected to node 1 for the 4-bus system, one ESS connected to node 17 and 33 for the 33-bus system, and one ESS connected to node 2 and 12 for the 69-bus system, respectively.

The capacity of ESS in the 4-bus system is 1.5 MWh. The bound on the quantity of electric charge is [0.15, 1.5] MWh. Both the maximum charge and discharge power are 150 kW.

The capacity of ESS connected to node 17 in the 33-bus system and node 2 in the 69-bus system is 1.5 MWh. The bound on the quantity of electric charge is [0.15, 1.5] MWh. Both the maximum charge and discharge power are 300 kW.

The capacity of ESS connected to node 33 in the 33-bus system and node 12 in the 69-bus system is 0.5 MWh. The bound on quantity of electric charge is [0.05, 0.5] MWh. Both the maximum charge and discharge power are 100 kW.

The charge and discharge efficiency of each ESS is 0.9. The maximum cycle of ESS is set to be 3. The action costs of OLTC, SCR, and ESS, that is c^{OLTC}, c_l^{SCR}, and c_l^{ESS}, are set to be 80, 40, and 50 \$/MWh, respectively.

The electricity price, normalized predicted load, and wind power of each time period are shown in Table I. The maximum predicted load in nodes 2~4 for the 4-bus system is 1 MW. The power factor is 0.95. The maximum predicted power of each wind turbine in the 4-, 33-, and 69-bus systems are 2.5, 0.25, and 0.25 MW, respectively.
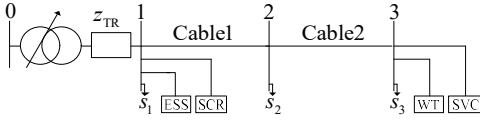
Fig. 3.   Topology of the 4-bus distribution system.

TABLE I
ELECTRICITY PRICE, LOAD, AND WIND POWER

Time	Price ($/MWh)	Load (%)	Wind (%)	Time	Price ($/MWh)	Load (%)	Wind (%)
1	50	65.8	82.7	13	78	80	9.2
2	38	63.2	68.7	14	85	75.3	1.3
3	39	62.1	85.3	15	100	83.2	2.0
4	40	62.6	94.6	16	82	84.2	0
5	46	62.9	100	17	70	84.7	3.9
6	45	63.6	91.2	18	115	90.5	9.7
7	145	70.5	89.1	19	160	100	36.2
8	150	75.3	79.8	20	200	95.8	45.9
9	64	77.9	75.4	21	220	93.7	36.4
10	60	84.2	48.2	22	210	89.5	43.7
11	64	85.3	29.0	23	60	80.0	46.5
12	75	84.7	21.2	24	40	72.1	33.7

5.2 Simulation Results

For the three systems, the optimization results of turn ratio for OLTC at different time periods and prediction errors are the same, all of which are 1.06. For the 4-bus system, the optimization results of compensated reactive power for SCR at different time periods and prediction errors are the same, all of which are -0.3 Mvar. For the 33- and 69-bus system, the optimization results of compensated reactive power for SCR at different time periods and prediction errors are the same, all of which are 0.6 Mvar.

For the 4-bus system, the charging and discharging power at different time periods are shown in Fig. 4. When the electricity price is minimum during the time period 2:00~4:00, the ESS is charged with the maximum power. When the electricity price is maximum during the time period 20:00~22:00, the ESS is discharged with the maximum power.

The charging and discharging states of ESS are shown in Fig. 5. When the charging power is high, the charging state equals 1 while the discharging state equals 0. When the discharging power is high, the charging state equals 0 while the discharging state equals 1. Further, the sum of charging and discharging states must be no more than 1.
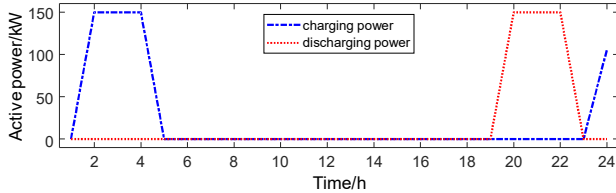

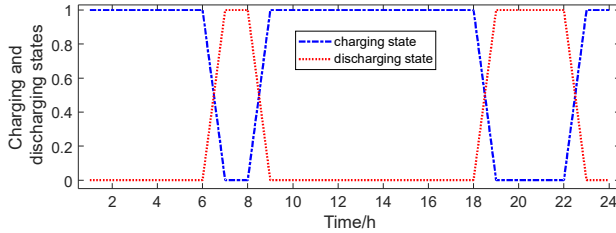Fig. 4.   Charging and discharging power of ESS of the 4-bus system.

Fig. 5.   Charging and discharging states of ESS of the 4-bus system.

The maximum gap of conic relaxation is shown in Table II. As can be seen, the gap of each case is smaller than 5e-6, which implies that the conic relaxation is actually exact to the

original non-convex model.

TABLE II
MAXIMUM GAP OF CONIC RELAXATION

ζ	4-bus system	33-bus system	69-bus system
0.1	2.6482e-8	1.1511e-8	1.6303e-6
0.2	8.7915e-8	1.1682e-8	1.8231e-6
0.3	5.0155e-8	1.1737e-8	3.9148e-6
0.4	1.4872e-7	1.1835e-8	2.2381e-6
0.5	3.6849e-8	1.1859e-8	4.0481e-6
0.6	6.0642e-8	1.1916e-8	3.7460e-6

5.3 Comparison of Computational Performance Between the Proposed and CCG Method

Using the proposed method in Section 4.2 and the improved CCG method (the sub-problem is modeled and solved using the proposed method in this paper), the objective function values of the mater and sub-problem, iterations, and computational time for the 4- and 33-bus system are shown in Tables III~VI. As can be seen, the objective function values of the proposed method fit that of the improved CCG method very well for different prediction errors. Thus, the precision of the proposed method is relatively high. However, the computational rate of the proposed method is faster than the improved CCG method for all the cases except when the prediction error equals 0.6 for the 4-bus system. Further, in all the cases, the proposed method can converge within only 2 iterations.

Fig. 6 shows the electricity costs of the main grid for master and sub-problem during iteration for the 33-bus system when the prediction error is 0.2. As can be seen, the proposed algorithm only needs 2 iterations to converge where the upper bound keeps constant and the lower bound is increasing. The program stops until the gap between the upper and lower bound is smaller than the given value.

TABLE III
OBJECTIVE FUNCTION VALUES FOR 4-BUS NETWORK

ζ	Objective function (thousand dollars)			
	Improved CCG		Proposed method	
	MP	SP	MP	SP
0.1	4.0100	3.9470	4.0100	3.9470
0.2	4.8264	4.7635	4.8264	4.7635
0.3	5.6484	5.5854	5.6484	5.5854
0.4	6.4760	6.4130	6.4760	6.4130
0.5	7.3094	7.2464	7.3094	7.2464
0.6	8.1489	8.0859	8.1489	8.0859

TABLE IV
ITERATIONS AND COMPUTATIONAL TIME FOR 4-BUS NETWORK

ζ	Improved CCG		Proposed method	
	Iterations	Time (s)	Iterations	Time (s)
0.1	2	53.783	2	43.807
0.2	2	51.381	2	37.475
0.3	2	58.444	2	34.498
0.4	2	58.405	2	43.756
0.5	2	55.162	2	44.109
0.6	2	234.239	2	268.439

Using the proposed method and the CCG method in [8], the objective function values of mater and sub-problem, iterations, and computational time for the 69-bus system are shown in Table VII and VIII. As can be seen, the objective function values of the proposed method are lower than that of the CCG method for different prediction errors. This is because the number of variables and constraints of the CCG method is much larger than the proposed method. For the same relative dual gap, the precision of the former is lower than the latter. Moreover, although the scale of the problem is very large, the proposed method only needs less than 650 seconds and 2 iterations. Nevertheless, the CCG method needs about 6,095~8,010 seconds and reaches the maximum iterations 7.

Therefore, the computational speed of the proposed method is much faster than the CCG method. Furthermore, the proposed method needs much less memory than the CCG method.

TABLE V
OBJECTIVE FUNCTION VALUES FOR 33-BUS NETWORK

ζ	Objective function ((thousand dollars))			
	Improved CCG		Proposed method	
	MP	SP	MP	SP
0.1	6.3069	6.1391	6.3069	6.1391
0.2	7.0422	6.8743	7.0422	6.8743
0.3	7.9154	7.7475	7.9154	7.7475
0.4	9.0912	8.9233	9.0912	8.9233
0.5	10.0154	9.8475	10.0156	9.8475
0.6	11.0535	10.8798	11.0536	10.8798

TABLE VI
ITERATIONS AND COMPUTATIONAL TIME FOR 33-BUS NETWORK

ζ	Improved CCG		Proposed method	
	Iterations	Time (s)	Iterations	Time (s)
0.1	2	222.728	2	155.649
0.2	2	220.986	2	154.633
0.3	2	222.238	2	146.274
0.4	2	221.467	2	153.368
0.5	2	221.942	2	154.222
0.6	2	247.540	2	149.922

TABLE VII
OBJECTIVE FUNCTION VALUES FOR 69-BUS NETWORK

ζ	Objective function ((thousand dollars))			
	CCG		Proposed method	
	MP	SP	MP	SP
0.1	6.8862	6.7195	6.8394	6.6743
0.2	7.6412	7.4762	7.5821	7.4170
0.3	8.5639	8.3920	8.3356	8.1705
0.4	9.5894	9.4224	9.2259	9.0609
0.5	9.9721	9.8074	9.9080	9.7429
0.6	11.4549	11.2901	10.7125	10.5474

TABLE VIII
ITERATIONS AND COMPUTATIONAL TIME FOR 69-BUS NETWORK

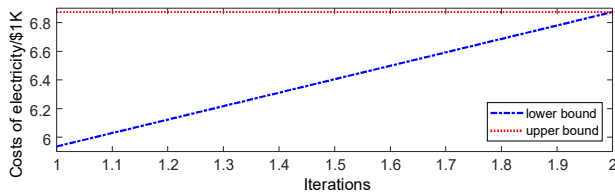| ζ	CCG		Proposed method	
	Iterations	Time (s)	Iterations	Time (s)
0.1	7	6095.892	2	633.078
0.2	7	7730.409	2	638.009
0.3	7	7812.867	2	633.229
0.4	7	7945.767	2	620.362
0.5	7	7998.384	2	632.997
0.6	7	8010.235	2	647.081

Fig. 6.   Iterations of the 33-bus distribution system.

VI   Conclusions

Generally, the shunt capacitor of coaxial cable cannot be ignored. In this paper, considering the action costs of regulating equipment, active and reactive power regulation capability of DG, a two-stage multi-period mixed-integer SOCP method is developed based on branch flow equations of radial distribution network with cables for coordinated optimization of active and reactive power. The proposed method aims to find a robust optimal solution that can hedge against any possible realization within the uncertain wind power output. Then a method that can iteratively solve the first- and second-stage model on cutting plane is proposed, in which the number of constraints and variables keeps constant during iteration. Further, the sub-problem only needs to be solved for each time period and then their results are accumulated. As an outcome, the computational rate of the proposed method without compromising precision is much higher than the traditional CCG method.
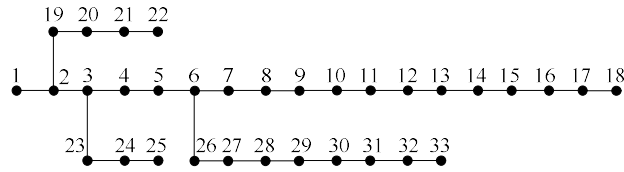
APPENDIX
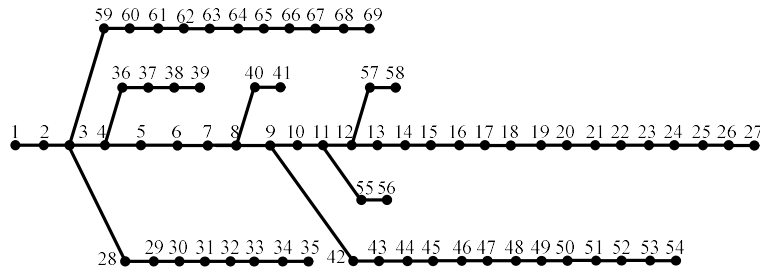Please find the appendix in the extended version [21].

REFERENCES

[1] M. Farivar, C. R. Clarke, S. H. Low, and K. M. Chandy, "Inverter VAR control for distribution systems with renewables," in *Proc. IEEE Int. Conf. Smart Grid Commun.*, Brussels, Belgium, Oct. 2011, pp. 457–462.

[2] J. Zhang, M. Cui, B. Li, H. Fang, and Y. He, "Fast solving method based on linearized equations of branch power flow for coordinated charging of EVs (EVCC)," *IEEE Trans. Veh. Technol.*, vol. 68, no. 5, pp. 4404–4418, May 2019.

[3] H. Gao, J. Liu, and L. Wang, "Robust coordinated optimization of active and reactive power in active distribution systems," *IEEE Trans. Smart Grid*, vol. 9, no. 5, pp. 4436–4447, 2017.

[4] Q. Nguyen, H. V. Padullaparti, K.-W. Lao, S. Santoso, X. Ke, and N. Samaan, "Exact optimal power dispatch in unbalanced distribution systems with high PV penetration," *IEEE Trans. Power Syst.*, vol. 34, no. 1, pp. 718–728, 2019.

[5] B. A. Robbins, H. Zhu, and A. D. Domínguez-García, "Optimal tap setting of voltage regulation transformers in unbalanced distribution systems," *IEEE Trans. Power Syst.*, vol. 31, no. 1, pp. 256–267, 2016.

[6] E. Dall'Anese, H. Zhu, and G. B. Giannakis, "Distributed optimal power flow for smart microgrids," *IEEE Trans. Smart Grid*, vol. 4, no. 3, pp. 1464–1475, 2013.

[7] N. Li, L. J. Chen, and S. H. Low, "Exact convex relaxation of OPF for radial networks using branch flow model," in *Proc. IEEE 3rd Int. Conf. Smart Grid Commun.*, Tainan, Taiwan, Nov. 2012, pp. 7–12.

[8] J. Lavaei and S. H. Low, "Zero duality gap in optimal power flow problem," *IEEE Trans. Power Syst.*, vol. 27, no. 1, pp. 92–107, 2012.

[9] J. Lavaei, D. Tse, and B. Zhang, "Geometry of power flows and optimization in distribution networks", *IEEE Trans. Power Syst.*, vol. 29, no. 2, pp. 572–583, Mar. 2014.

[10] L. Gan, N. Li, U. Topcu, and S. H. Low, "Exact convex relaxation of optimal power flow in radial networks," *IEEE Trans. Autom. Control*, vol. 60, no. 1, pp. 72–87, 2015.

[11] M. Farivar and S. H. Low, "Branch flow model: Relaxations and convexification—Part I," *IEEE Trans. Power Syst.*, vol. 28, no. 3, pp. 2554–2564, 2013.

[12] M. Farivar and S. H. Low, "Branch flow model: Relaxations and convexification—Part II," *IEEE Trans. Power Syst.*, vol. 28, no. 3, pp. 2565-2572, 2013.

[13] M. Nick, R. Cherkaoui, J. L. Boudec, and M. Paolone, "An exact convex formulation of the optimal power flow in radial distribution networks including transverse components," *IEEE Trans. Autom. Control*, vol. 63, no. 3, pp. 682-697, 2018.

[14] Y. Xiang, J. Liu, and Y. Liu, "Robust energy management of microgrid with uncertain renewable generation and load," *IEEE Trans. Smart Grid*, vol. 7, no. 2, pp. 1034–1043, Mar. 2016.

[15] C. Lee, C. Liu, S. Mehrotra, and Z. Bie, "Robust distribution network reconfiguration," *IEEE Trans. Smart Grid*, vol. 6, no. 2, pp. 836–842, Mar. 2015.

[16] T. Ding, C. Li, Y. Yang, J. Jiang, Z. Bie, and F. Blaabjerg, "A two-stage robust optimization for centralized-optimal dispatch of photovoltaic inverters in active distribution networks," *IEEE Trans. Sustain. Energy*, vol. 8, no. 2, pp. 744-754, 2017.

[17] T. Ding, S. Liu, W. Yuan, Z. Bie, and Bo Zeng, "A two-stage robust reactive power optimization considering uncertain wind power integration in active distribution networks," *IEEE Trans. Sustain. Energy*, vol. 7, no. 1, pp. 301-311, 2016.

[18] B. Zeng and L. Zhao, "Solving two-stage robust optimization problems using a column-and-constraints generation method," *Operations Research Letters*, vol. 41, no. 5, pp. 457-461, 2013.

[19] M. E. Baran and F. F. Wu, "Optimal capacitor placement on radial distribution systems," *IEEE Trans. Power Del.*, vol. 4, no. 1, pp. 725–734, Jan. 1989.

[20] M. E. Baran and F. F. Wu, "Optimal sizing of capacitors placed on a radial distribution system," *IEEE Trans. Power Del.*, vol. 4, no. 1, pp. 735–743, Jan. 1989.

[21] https://www.techrxiv.org/articles/preprint/Multi-period_Fast_Robust_Optimization_of_Distribution_System_With_Cables/12613817

APPENDIX A

19 20 21 22

1 2 3 4 5 6 7 8 9 10 11 12 13 14 15 16 17 18

23 24 25 26 27 28 29 30 31 32 33

33-bus distribution network

APPENDIX B

59 60 61 62 63 64 65 66 67 68 69

36 37 38 39   40 41   57 58

1 2 3 4 5 6 7 8 9 10 11 12 13 14 15 16 17 18 19 20 21 22 23 24 25 26 27

55 56

28 29 30 31 32 33 34 35 42 43 44 45 46 47 48 49 50 51 52 53 54

69-bus distribution network

APPENDIX C

SHUNT CAPACITOR OF 33-BUS DISTRIBUTION SYSTEM

branch	C/ F	branch	C/ F	branch	C/ F
1	0	12	2.0740e-7	23	5.1650e-7
2	7.8740e-8	13	1.9350e-6	24	1.1880e-6
3	4.2067e-7	14	1.1943e-6	25	1.1746e-6
4	3.1228e-7	15	8.8120e-7	26	1.7323e-7
5	3.2518e-7	16	9.1305e-7	27	2.4242e-7
6	1.1844e-6	17	2.8832e-6	28	1.5642e-6
7	1.0367e-6	18	9.6163e-7	29	1.1737e-6
8	3.9387e-7	19	2.6219e-7	30	4.3307e-7
9	1.2397e-6	20	2.2707e-6	31	1.6133e-6
10	1.2397e-6	21	8.0147e-7	32	6.0630e-7
11	1.0890e-7	22	1.5703e-6	33	8.9830e-7

APPENDIX D

SHUNT CAPACITOR OF 69-BUS DISTRIBUTION SYSTEM

branch	C/ F	branch	C/ F	branch	C/ F
1	0	24	1.9182e-7	47	4.4061e-7
2	2.0104e-9	25	4.5987e-7	48	1.6854e-7
3	2.0104e-9	26	1.7105e-7	49	1.9635e-7
4	6.03114e-9	27	9.5828e-8	50	4.3307e-7
5	4.92544e-8	28	1.8093e-8	51	8.3096e-8
6	3.1228e-7	29	2.6219e-7	52	1.2364e-7
7	3.2518e-7	30	2.2030e-7	53	6.0630e-7
8	7.8740e-8	31	3.8867e-8	54	8.8825e-7
9	4.2050e-8	32	1.9434e-7	55	1.0236e-7

10	4.5351e-7	33	4.7177e-7	56	2.3454e-9
11	1.1576e-7	34	9.4588e-7	57	4.0945e-7
12	3.9387e-7	35	7.8287e-7	58	2.6805e-9
13	5.6961e-7	36	1.4073e-8	59	1.8093e-8
14	5.7798e-7	37	3.4897e-7	60	2.6219e-7
15	5.8569e-7	38	1.1880e-6	61	2.0606e-7
16	1.0890e-7	39	3.3691e-7	62	5.9474e-7
17	2.0740e-7	40	7.9242e-8	63	3.5182e-9
18	2.6805e-9	41	1.8663e-7	64	1.4255e-6
19	1.8144e-7	42	1.4843e-7	65	6.06976e-7
20	1.1660e-7	43	1.7323e-7	66	8.0080e-8
21	1.8914e-7	44	2.4242e-7	67	1.9434e-8
22	7.7064e-9	45	2.4007e-7	68	2.3002e-7
23	8.8122e-8	46	8.9412e-7	69	2.0104e-9